Synchronization modes of triple flickering buoyant diffusion flames: Experimental identification and model interpretation

Yicheng Chi,[1,*] Zeying Hu,[1,*] Tao Yang,[2] and Peng Zhang[1,†]
[1]*Department of Mechanical Engineering, City University of Hong Kong, Kowloon Tong, Hong Kong*
[2]*Department of Mechanical Engineering, The Hong Kong Polytechnic University, Hung Hom, Hong Kong*

(Received 12 August 2023; revised 18 November 2023; accepted 18 January 2024; published 15 February 2024)

The synchronization modes of a nonlinear oscillator system consisting of three identical flickering buoyant diffusion flames in isosceles triangles were studied experimentally and theoretically. Five synchronization modes, such as the in-phase, flickering death, partially flickering death, partially in-phase, and rotation modes, were experimentally observed and identified by systematically adjusting the flame distance and fuel flow rates. Two toy models were adopted to interpret the experimentally identified dynamical modes: one is the classical Kuramoto model, and the other is a complexified Stuart-Landau model, which was proposed through the introduction of the complex coupling term. The theoretical results show that the Kuramoto model successfully interpreted the dynamical modes except for those associated with amplitude death, and the complexified Stuart-Landau model well interpreted all the dynamical modes identified in our experiment. Remarkably, the proposed complexified Stuart-Landau model breaks a new path in the investigation of globally coupled nonlinear dynamical systems with identical oscillators, especially for the study of amplitude death mode.

DOI: 10.1103/PhysRevE.109.024211

I. INTRODUCTION

Nonlinear dynamics of coupled oscillators is a long-lasting problem in the study of complex systems [1,2], which has gained increasing attention in recent years. Flickering buoyant diffusion flames can be treated as a type of nonlinear oscillator due to its inherent characteristics. The flame flicker of Bunsen-type diffusion flame exhibits vibratory motion with a frequency of about 10 Hz was reported by Chamberlin and Rose [3]. A similar phenomenon using a Burke-Schumann diffusion flame was observed by Barr [4], who described "the vibration is seen to consist of a progressive necking of the flame which can lead to the formation of a flame bubble which burns itself out separated from the anchored flame". Such flame phenomena can be observed in pool fires [5,6] and also in premixed and partially premixed flames [7,8]. It is worth emphasizing that Chen *et al.* [9] the prominent experimental work by Chen *et al.* [9] for flow visualization of a jet diffusion flame proved that the flickering flame is a self-exciting flow oscillation because the small vortices within the luminous flame originate from Kelvin-Helmholtz (hereinafter referred to as *K-H*) instability of the fuel jet and the large toroidal vortices outside the luminous flame originate from the buoyance-induced *K-H* instability. More recent theoretical works [10,11] revealed that the flame flicker is essentially a flow of global instability.

Multiple flickering flames have been used to constitute nonlinear dynamical systems of flame oscillators. Interesting dynamical modes of two candle flames were reported by Kitahata *et al.* [12] who observed two distinct dynamical modes using, such the in-phase mode (two flames flicker synchronously with no phase difference) and the antiphase mode (two flames flicker alternatively with a phase-shift of π). Forrester [13] and Manoj *et al.* [14] reported a similar phenomenon in candle flames. Besides, Manoj *et al.* [14] also observed the amplitude death mode, in which the two flames cease to oscillate. Recently, Ju *et al.* [15] suppressed the flame flickering by dynamically adjusting the flame distance. The flow visualization of Dange *et al.* [16] showed that the interaction between buoyance-induced vortices plays a significant role in producing different dynamical modes. The vortex-dynamical mechanism of coupled dual flames was also verified by the PIV velocity measurement of Fujisawa *et al.* [17] of pipe-burner diffusion flames and by the observations of Bunkwang *et al.* [18,19] in methane-air jet diffusion flames. This vortex-dynamical mechanism has also been substantiated by the numerical simulations of Yang *et al.* [20] for pool flames, Bunkwang *et al.* [18] for buoyant jet flames, and Tokami *et al.* [21] for buoyancy-induced turbulent diffusion flames.

Larger systems of flickering buoyant diffusion flames give rise to richer dynamical phenomena. Okamoto *et al.* [22] discovered four distinct dynamical modes, such as the in-phase, death, rotation, and partially in-phase modes, by using three flickering candle flames in an equilateral triangle arrangement. Yang *et al.* [23] computationally reproduced these four modes and interpreted them from the perspective of vortex interaction and particularly of vorticity reconnection and vortex-induced flow. Very recently, Chi *et al.* [24] developed a Wasserstein-space-based methodology for the mode recognition of coupled triple flickering flames. Some typical dynamical modes of the triple flickering flames have been

*These authors contributed equally to the work.
†Corresponding author: penzhang@cityu.edu.hk

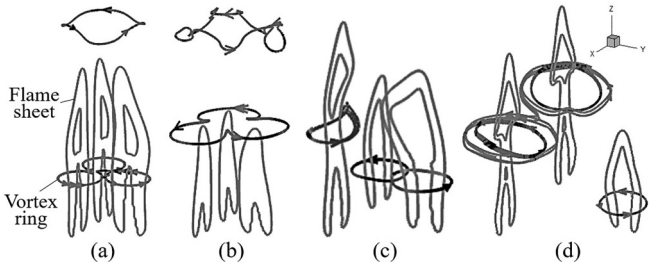

FIG. 1. Schematic of the vortex interaction in triple flickering flames [23]: (a) in-phase mode, (b) flickering death mode, (c) rotation mode, and (d) partially in-phase mode.

explained by the interaction of toroidal vortices [23], as illustrated in Fig. 1. The in-phase mode occurs when the three toroidal vortices merge into a trefoil vortex, which grows up and sheds off to pinch off the flame. When the trefoil vortex sheds off the downstream of the flame, the flame is not pinched and the flickering death mode occurs. The rotation mode occurs when the three toroidal vortices do not merge but shed off alternatively from each flame. The partially in-phase mode is due to the merging of two toroidal vortices into a "∞"-shape vortex, which results in the in-phase flickering of two flames but has a phase difference of π with the third vortex.

Forrester [13] experimentally observed an initial-arch-bow-initial "worship" oscillation mode for four candle flames in a square arrangement and conjectured the existence of a chimera state [25], which is characterized by the hybrids of synchronized and desynchronized flames. Manoj *et al.* [26] investigated the coupled four flickering candle flames in a rectangle arrangement and observed the clustering mode, in which the flames separate into two clusters of synchronized flames, the chimera mode, in which the flames separate into synchronized and desynchronized groups of flames, and the weak chimera mode, in which three frequency-synchronized flames coexist with one desynchronized flame. Recently, Manoj *et al.* [27] experimentally investigated the coupled behavior of annular networks with 5–7 candle-flame oscillators and observed variants of clustering and chimera states depending on the inter-flame distance and number of flames in the network. In addition, Chen *et al.* [28] studied the dynamical characteristics of nonidentical asymmetric candle flames.

Compared with the many experimental and computational studies on multiple flickering flame systems, very few studies attempted to establish a dynamical model to interpret the experimental findings. By hypothesizing that a lack of oxygen is a key factor in producing the flickering flame and that the thermal radiation coupling causes the synchronization of two flames, Kitahata *et al.* [12] proposed a phenomenological model to interpret their experiments. The radiation measurement of Gergely *et al.* [29] did not support the radiation coupling hypothesis, and they hypothesized that the oxygen flow induced by the thermal expansion is responsible for the flame coupling and proposed a modified phenomenological model. In addition, Manoj *et al.* adopted a toy-model approach where the time-delay coupled identical Stuart-Landau oscillators were used to reproduce the dynamical modes of two [14] and four [26] coupled candle flames.

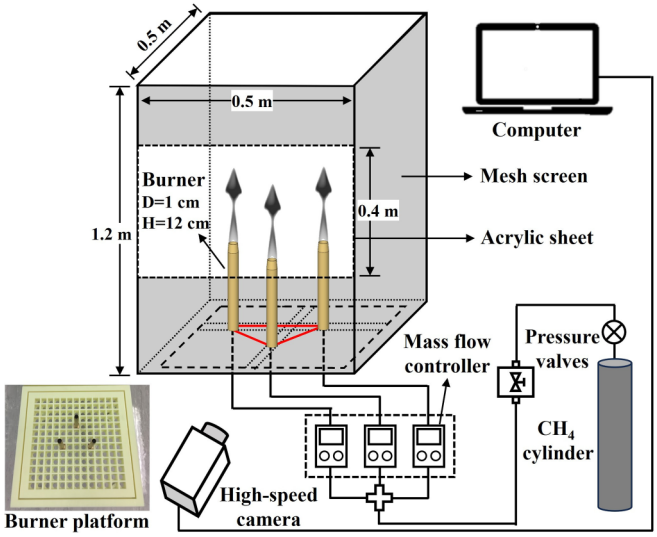

FIG. 2. Schematic and photograph of the experimental apparatus consisting of burners, fuel flow controls, and visualization systems.

Although the mechanism of a single flickering flame is well understood [30–32], the collective dynamical behaviors of coupled multiple flickering flames are complex and inadequately understood. Such a complex system differs from the system that can be studied by decomposition, because the entirety is not equal to the sum of parts and the collective behaviors are not simply linear superposition of the coupled flames. Therefore, for studying the complex dynamical system of coupled multiple flickering flames, the major challenges are dynamical mode recognition and dynamical model establishment.

The present study was motivated by the above challenges and focused on establishing a nonlinear dynamical model of a coupled triple flickering flames system because it can be treated as the smallest nontrivial multiple-flame system. We adopted Bunsen-type burners to produce flickering buoyant diffusion flames at a well-controlled gas-fuel experimental platform and systematically investigated three flickering flames in the isosceles triangle arrangement conducted by varying three physical parameters, the leg (L) and the base (B) of the triangle, and the flow rate (Q) for each flame. Considering the complex flow of multiple coupled flickering flames is not well understood, we did not adopt the approach of establishing phenomenological models. Instead, we attempted to establish toy models based on the Kuramoto model and the Stuart-Landau model, to retain the essential features of the complex system of multiple coupled flickering flames.

II. METHODOLOGY

A. Experiment setup

The experimental setup is sketched in Fig. 2 for a triple flickering flame system. Each flickering flame was produced by a brass Bunsen-type burner with 12 cm in height (H) and 1 cm in diameter (D) and the nozzle outlet was pinched slightly to reduce the influence of tube thickness. The flames were in an isosceles triangle arrangement by varying the leg (L) in the range of 2.0–10.8 cm and the base (B) in the range

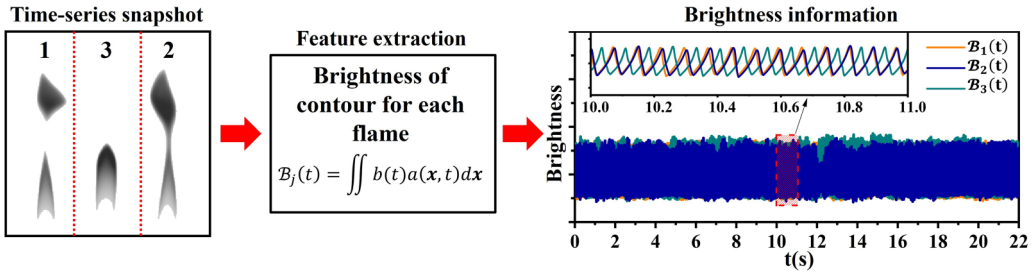

FIG. 3. Flowchart of the feature extraction process from experiment snapshots to brightness signal.

of 4.0–8.0 cm (the two base flames and the vertex flame are denoted by flame 1, flame 2, and flame 3, respectively) for a systematical parametric study. The limiting arrangements, such as the straight line arrangement ($B/L = 2$) and the equilateral triangle arrangement ($B/L = 1$), were also considered in the experiment. The chessboard-type burner platform was designed to better support and adjust the burners. Methane (99.9% purity) was employed in the experiment and was accurately controlled by a mass flow controller (Alicat Scientific, MC-5SLPM-D/5M) in the flow rate (Q) range of 0.45–0.65 standard liter per minute (slpm). The experimental snapshots of the flickering flames were recorded by a high-speed camera (Kron Technologies, Chronos 2.1-HD) with a 105 mm UV lens and at a frame rate of 500 fps (frame per second). To establish a stable and consistent experimental environment, fire-proof curtains and mesh screens were used to minimize the external disturbance, and the experiments were carried out at 1 atm and 25°. Besides, it should be noted that each trial was recorded continuously for 22 seconds of fully developed flames. Each case was carried out multiple times to ensure experimental repeatability.

B. Physics-informed dimensionality reduction

The present dynamical system is infinite-dimensional in nature and is governed by a series of partial differential equations (PDEs) of temperature (T), pressure (P), velocity ($\boldsymbol{v}$), and molar fractions of species (Y_i) describing the time-space evolution of the chemically reacting flow. The physics-informed dimensionality reduction is to choose an appropriate characteristic physical quantity to retain the essential characteristic of a flickering flame, which is the periodicity of its characteristic physical quantities. As a result, ordinary differential equations instead of PDEs can be applied to describe the dynamical behaviors of the triple-flame system.

Many quantities of the flame can be selected as characteristic features. For example, the pressure, temperature, or luminosity of the flickering flame at a certain height can be considered as the local information of the flickering flames [33,34]; the information of flame morphology, such as flame height, size, and brightness, can be considered as global information of the flickering flames [17,29,35]. In the present study, we adopted the previous approach where the integral brightness information was obtained directly from the experimental high-speed snapshots [24].

As shown in Fig. 3, a grayscale snapshot at the time t was divided into three parts, each of which contains only one of the three flames. The brightness of each pixel of the snapshot is represented by an integer $b(t)$ between 0 (pure black) and 255 (pure white). A truncation value of $b_0 = 50$ was used to obtain the "area of flame" function for each flame,

$$a(\boldsymbol{x}, t) = 1 \text{ for } b \geqslant b_0;\ a(\boldsymbol{x}, t) = 0 \text{ otherwise},$$

which is equivalent to the Otsu [29,36–38] method for binarizing grayscale images. The flame brightness is calculated by

$$\mathcal{B}_j(t) = \iint b(t)a(\boldsymbol{x}, t)d\boldsymbol{x}. \tag{1}$$

Therefore, the dynamical feature in the triple flickering flame system at a certain time instant t can be represented by $\mathcal{B}_j(t)$, $(j = 1, 2, 3)$ of three parts.

For the convenience of the analysis, we unified the amplitude of the brightness of each flickering flame. The characteristic quantity of brightness can be normalized as

$$\tilde{\mathcal{B}}_j(t) = \frac{\mathcal{B}_j(t) - \bar{\mathcal{B}}_j(t)}{\bar{\mathcal{B}}_j(t)}, \tag{2}$$

where $\bar{\mathcal{B}}_j(t)$ denotes the average value of brightness for each flickering flame during 22 s in the present study. In this way, the fluctuation of normalized brightness $\tilde{\mathcal{B}}_j(t)$ can be centered on zero.

C. Hilbert transform

The Hilbert transform [39] was adopted to process the normalized brightness information obtained in Sec. II B to acquire two essential features (instantaneous amplitude and phase difference) of the individual flickering flame. The Hilbert transform is a type of singular integral that takes a set of real-valued signals $\tilde{\mathcal{B}}(t)$ and then produces another set of transformed signals $\tilde{\mathcal{B}}_H(t)$, which is the convolution of $\tilde{\mathcal{B}}(t)$ with the signal function $1/\pi t$. The Hilbert transform of $\tilde{\mathcal{B}}(t)$ is given by

$$\tilde{\mathcal{B}}_H(t) = \frac{1}{\pi} P.V. \int_{-\infty}^{\infty} \frac{\tilde{\mathcal{B}}(\tau)}{t - \tau} d\tau, \tag{3}$$

where $P.V.$ is the Cauchy principal value. A complex signal $\zeta(t)$ can be defined by its parts: one is the real part $\tilde{\mathcal{B}}(t)$ and another is the imaginary part $\tilde{\mathcal{B}}_H(t)$,

$$\zeta(t) = \tilde{\mathcal{B}}(t) + i\tilde{\mathcal{B}}_H(t) = A(t)e^{i\theta(t)}, \tag{4}$$

where $A(t)$ and $\theta(t)$ are the amplitude and phase, respectively. Therefore, the relative phase difference between any two

signals can be expressed as

$$\varphi_{jk}(t) = \theta_j(t) - \theta_k(t), \tag{5}$$

where $\theta_j(t)$ and $\theta_k(t)$ are the instantaneous phase of the oscillators j and k, respectively.

D. Kuramoto model

Synchronization phenomena attracted a great deal of interest in physics and relevant fields and are still a very active area of research with many unresolved problems since the seminal work of Winfree in the 1960s [40]. One of the most successful models in the interpretation of the phenomena is the Kuramoto model [41], which has a wide range of applications, such as in flashing fireflies [42], circadian rhythms [43], neuronal networks [44], and power-grid networks [45]. The dynamical modes of multiple coupled flickering flames are typical synchronization phenomena. Therefore, we adopted the classical Kuramoto model to interpret the collective behaviors of the flames that were observed in experiments. The Kuramoto model of the present problem is expressed as

$$\dot{\theta}_j(t) = \omega_j + \sum_{k=1}^{N} \frac{K_{jk}}{N} \sin[\theta_k(t) - \theta_j(t)], \tag{6}$$

where $\theta_j(t)$ is the instantaneous phase of the flame j at time t, $\dot{\theta}_j(t)$ is its time derivative, ω_j is the natural frequency of the jth flame oscillator, N is the number of oscillators, K_{jk} is a real number that represents the coupling strength between flame oscillators j and k.

E. Complexified Stuart-Landau model

The Stuart-Landau model, which is a canonical model for limited-cycle oscillation describing dynamics near supercritical Hopf bifurcation, has been widely used in describing synchronization in neural oscillators [46], electrochemical reaction oscillators [47,48], lasers [49], etc. The Stuart-Landau equation for the present problem is given by

$$\dot{z}_j(t) = f_j[z_j(t)] + \sum_{k=1}^{N}(K_{jk} + iK'_{jk})[z_k(t) - z_j(t)] + (\sigma + i\sigma')\epsilon(t), \tag{7}$$

where $z_j = \tilde{\mathcal{B}}_j(t) + i\tilde{\mathcal{B}}_j H(t) = r_j(t)e^{i\theta_j(t)}$ is the complex number representing the state of jth oscillator. In the present study, z_j corresponds to the complex brightness signal of each flame oscillator. $\epsilon(t)$ is the Gaussian white noise to mimic the unavoidable perturbation encountered in practical experiments and $\sigma + i\sigma'$ represents the strength of additional noise. The local dynamics $f_j(z_j(t))$ is expressed in the following form [41]:

$$f_j(z_j(t)) = [\alpha + i\omega_j - \beta|z_j(t)|^2]z_j(t), \tag{8}$$

where ω_j denotes the natural frequency of jth oscillator. α and β are real parameters associated with the amplitude.

It is worth emphasizing that the coupling strength in Eq. (7) is different from those widely used in the previous studies in the form $\sum_{k=1}^{N} K[z_k(t) - z_j(t)]$, where the coupling strength K is a real and positive number [47,48,50,51], and only a few exceptions introduced positive and negative [52] and the complex coupling strength [53]. Here, we considered the coupling strength a complex number, $K = K_{jk} + iK'_{jk}$, to describe the coupling strength between jth and kth flame oscillator, K_{jk} is the real part and K'_{jk} is the imaginary part.

The amplitude death mode was recognized as an emergent important phenomenon in globally coupled nonlinear dynamical systems, manifested by the complete suppression of oscillation and leading to stationarity, as a consequence of the interactions within the entire system [54]. In the theoretical framework of classical Stuart-Landau models, for the nonidentical oscillator, the occurrence of amplitude death mode is due to the intrinsic frequency mismatch [54–56]; whereas for the identical oscillator, the amplitude death mode was only reported in three scenarios: time-delay coupling [54,57–59], conjugate coupling [54,60,61], and nonlinear coupling [54]. In this work, we post a way to predict the amplitude death mode for the globally coupled nonlinear dynamical system with identical oscillators through the introduction of complex coupling strength in the classical Stuart-Landau model (known as the complexified Stuart-Landau model, as stated above). Consequently, the partially flickering death mode and flickering death mode observed in our experiment were successfully interpreted with this newly proposed model.

III. RESULTS AND DISCUSSION

A. Experimental results

Figures 4(a) and 4(b) show the experimental snapshots of seven distinct dynamical modes and the normalized brightness signal of each flickering flame, respectively. The brightness changes periodically with time and it is consistent with the periodic oscillation phenomena of the flickering flame. Here, the amplitude and phase difference information was used to distinguish the dynamical modes, and based on this we categorized these dynamical modes into seven. The criteria for the dynamical mode identification are summarized in Table I. Due to the possible noises and/or errors, the calculated phase difference between the flame oscillators cannot be perfectly zero (for in-phase mode), $2\pi/3$ (for rotation mode), or π (for antiphase mode). For the mode recognition based on phase difference, the tolerance of error of phase difference was set as $\pm 0.1\pi$. In fact, the average of standard deviations of phase difference for all synchronization modes is only 0.05π, which is sufficiently small to ensure the accuracy of dynamical mode identification.

Mode I: In-phase mode. The in-phase mode appears as the three flames flicker synchronously with a negligible phase difference (e.g., $B = 4.0$ cm, $L = 2.0$ cm, $Q = 0.50$ slpm). In the normalized brightness signal diagram, the time-averaged phase difference between each pair of flame oscillators is around 0, and the normalized amplitude of the three flame oscillators is nearly identical ($A_1 \approx A_2 \approx A_3 \neq 0, \varphi_{31} \approx 0.05\pi, \varphi_{32} \approx -0.03\pi, \varphi_{12} \approx -0.08\pi$) (See Movie 1 of the Supplemental Material [62]).

Mode II: Flickering death mode. The flickering death mode appears as the three flames cease to flicker periodically and the normalized amplitude of each flame is completely suppressed (e.g., $B = 6.0$ cm, $L = 3.0$ cm, $Q = 0.45$ slpm). In the normalized brightness signal diagram, the amplitude of all three

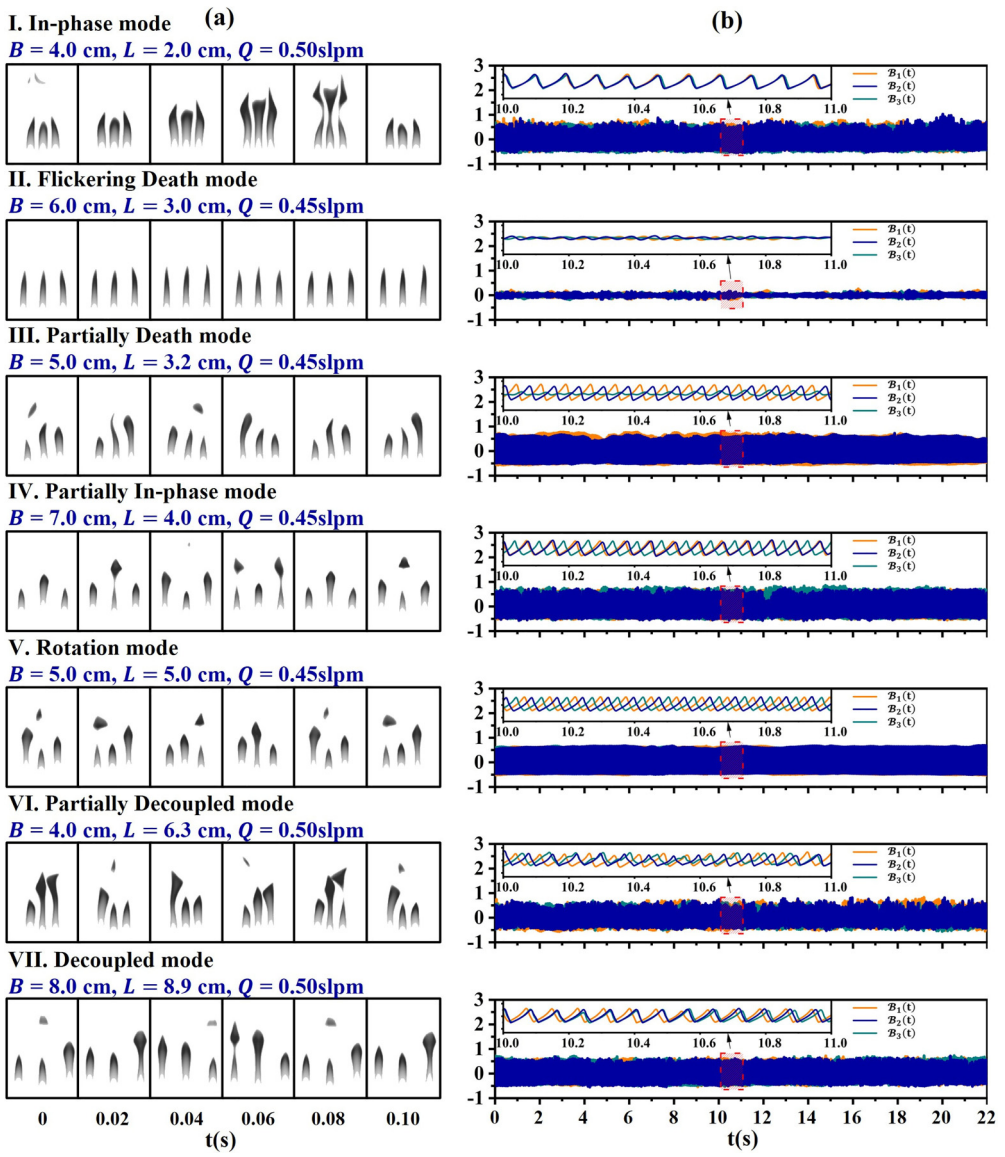

FIG. 4. (a) Experimental snapshots and (b) brightness signal diagrams for seven distinct dynamical modes in a triple-flickering buoyant diffusion flame system, which are I: the in-phase mode, II: the flickering death mode, III: the partially flickering death mode, IV: the partially in-phase mode, V: the rotation mode, VI: the partially decoupled mode, and VII: the decoupled mode, respectively.

flame oscillators fluctuated around zero ($A_1 \approx A_2 \approx A_3 \approx 0$). (See Movie 2 of the Supplemental Material [62]).

Mode III: Partially flickering death mode. The partially flickering death mode appears as flame 1 and flame 2 exhibit antiphase synchronization while flame 3 oscillates without the flame flicker. (e.g., $B = 5.0$ cm, $L = 3.2$ cm, $Q = 0.45$ slpm). In the normalized brightness signal diagram, the time-averaged phase difference between flame 1 and flame 2 is

TABLE I. Criteria for the dynamical mode identification.

Dynamical mode		Phase difference relationship	Amplitude value
Mode I	In-phase	$\varphi_1 - \varphi_2 = \varphi_2 - \varphi_3 = \varphi_3 - \varphi_1 = 0$	$A_1 = A_2 = A_3 \neq 0$
Mode II	Flickering death	Not applicable	$A_1 = A_2 = A_3 = 0$
Mode III	Partially death	$\varphi_1 - \varphi_2 = \pi$	$A_1 = A_2 \neq 0,\ A_3 = 0$
Mode IV	Partially In-phase	$\varphi_1 - \varphi_2 = 0,\ \varphi_3 - \varphi_1 = \varphi_3 - \varphi_2 = \pi$	$A_1 = A_2 \neq 0,\ A_3 \neq 0$
Mode V	Rotation	$\varphi_3 - \varphi_1 = \varphi_1 - \varphi_2 = \varphi_2 - \varphi_3 = 2\pi/3$	$A_1 = A_2 = A_3 \neq 0$
Mode VI	Partially decoupled	$\varphi_1 - \varphi_2 = \pi$	$A_1 = A_2 \neq 0,\ A_3 \neq 0$
Mode VII	Decoupled	No relationship between $\varphi_1,\ \varphi_2,\ \varphi_3$	$A_1 = A_2 = A_3 \neq 0$

around π, and the normalized amplitude of the brightness signal for flame 3 fluctuates around zero ($A_3 \approx 0,\ \varphi_{12} \approx 1.06\pi$). (See Movie 3 of the Supplemental Material [62]).

Mode IV: Partially in-phase mode. The partially in-phase mode appears as flame 1 exhibits in-phase synchronization with flame 2, but flame 3 exhibits antiphase synchronization with both flame 1 and flame 2 (e.g., $B = 7.0$ cm, $L = 4.0$ cm, $Q = 0.45$ slpm). In the normalized brightness signal diagram, the time-averaged phase difference between flame 1 and flame 2 is almost zero, while flame 3 is phase-shifted by around π ($\varphi_{31} \approx 1.08\pi,\ \varphi_{32} \approx 0.99\pi,\ \varphi_{12} \approx -0.09\pi$). (See Movie 4 of the Supplemental Material [62]).

Mode V: The rotation mode. The rotation mode appears as the three flames flicker in turns with a fixed phase difference when the three flames are arranged in an equal-lateral triangle (e.g., $B = 5.0$ cm, $L = 5.0$ cm, $Q = 0.45$ slpm). In the normalized brightness signal diagram, the time-averaged phase difference between each two flames is identical and around $2\pi/3$ ($\varphi_{13} \approx 0.72\pi, \varphi_{32} \approx 0.68\pi, \varphi_{12} \approx 0.60\pi$). (See Movie 5 of the Supplemental Material [62]).

Mode VI: The partially decoupled mode. The partially decoupled mode appears as if flame 1 and flame 2 are in an antiphase way while flame 3 flickers independently concerning flame 1 and flame 2 because it is sufficiently away from the two flames (e.g., $B = 4.0$ cm, $L = 6.3$ cm, $Q = 0.50$ slpm). In the normalized brightness signal diagram, it can be seen that flame 1 and flame 2 with an almost constant phase difference of π ($\varphi_{12} \approx 1.08\pi$). (See Movie 6 of the Supplemental Material [62]).

Mode VII: The decoupled mode. The decoupled mode occurs when the distance between the three flames is very large. Under this circumstance, the coupling strength between the flame oscillators is negligible (e.g., $B = 8.0$ cm, $L = 8.9$ cm, $Q = 0.50$ slpm). In the normalized brightness signal diagram, the phase difference is irregular ($\varphi_{21}, \varphi_{32}, \varphi_{13} \neq$ constant). (See Movie 7 of the Supplemental Material [62]).

On the other hand, we replotted the brightness information, as shown in Fig. 5, that can intuitively characterize the seven distinct dynamical modes of the triple flickering flames. For the in-phase mode (mode I), the three flames exhibit in-phase mode. The time interval of the results (10s ∼ 11s) was zoomed in, all three flame oscillators showed almost synchronized peaks (red bands) and troughs (blue bands). For the flickering death mode (mode II), we can see that the amplitudes of the three flames are nearly zero (green bands). For the partially flickering death mode (mode III), flame 1 and flame 2 exhibit antiphase synchronization that desynchronized peaks (red bands) and troughs (blue bands), and flame 3 remain stationary with a very small amplitude (green bands). For the partially in-phase mode (mode IV), flame 1 and flame 2 flicker synchronized for their patterns of color change are virtually identical, and flame 3 flickers asynchronously with flame 1 and flame 2. For the rotation mode (mode V), the three flames flicker alternatively where the patterns of color also change alternatively. For the partially decoupled mode (mode VI), we can only find that flame 1 and flame 2 always alternatively flicker, namely alternating peaks (red bands) and troughs (blue bands), and have no obvious change in a regular pattern of color with flame 3. For the decoupled mode (mode VII), the color patterns change between the three flames are irregular.

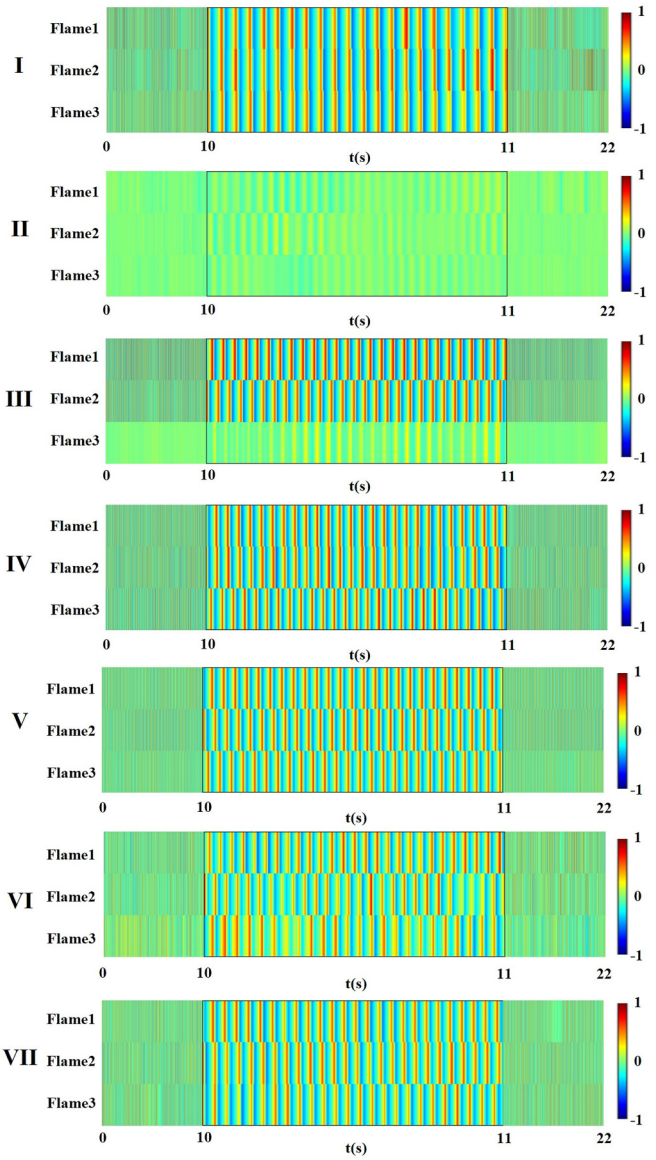

FIG. 5. Time traces (the time-varying brightness signal) of each flame oscillator for seven distinct dynamical modes in a triple-flickering buoyant diffusion flame system, which include I: the in-phase mode, II: the flickering death mode, III: the partially flickering death mode, IV: the partially in-phase mode, V: the rotation mode, VI: the partially decoupled mode, and VII: the decoupled mode, respectively.

B. Regime nomogram of dynamical modes

In the present study, we established a regime nomogram for a triple-flame system depending on the flame and geometric parameters, such as fuel flow rate (Q) and the leg (L) and the base (B) of the isosceles triangle. A wide range of parameters was studied to ensure comprehensive and systematic results for mode recognition of the triple flickering flames system, as shown in Fig. 6. Five fuel flow rates ($Q = 0.45$, 0.50, 0.55, 0.60, and 0.65 slpm) and four lengths of base ($B = 4$, 5, 6, 7, and 8 cm) with the change of lengths of the leg (L) for flames arrangement in the isosceles triangle were used, and

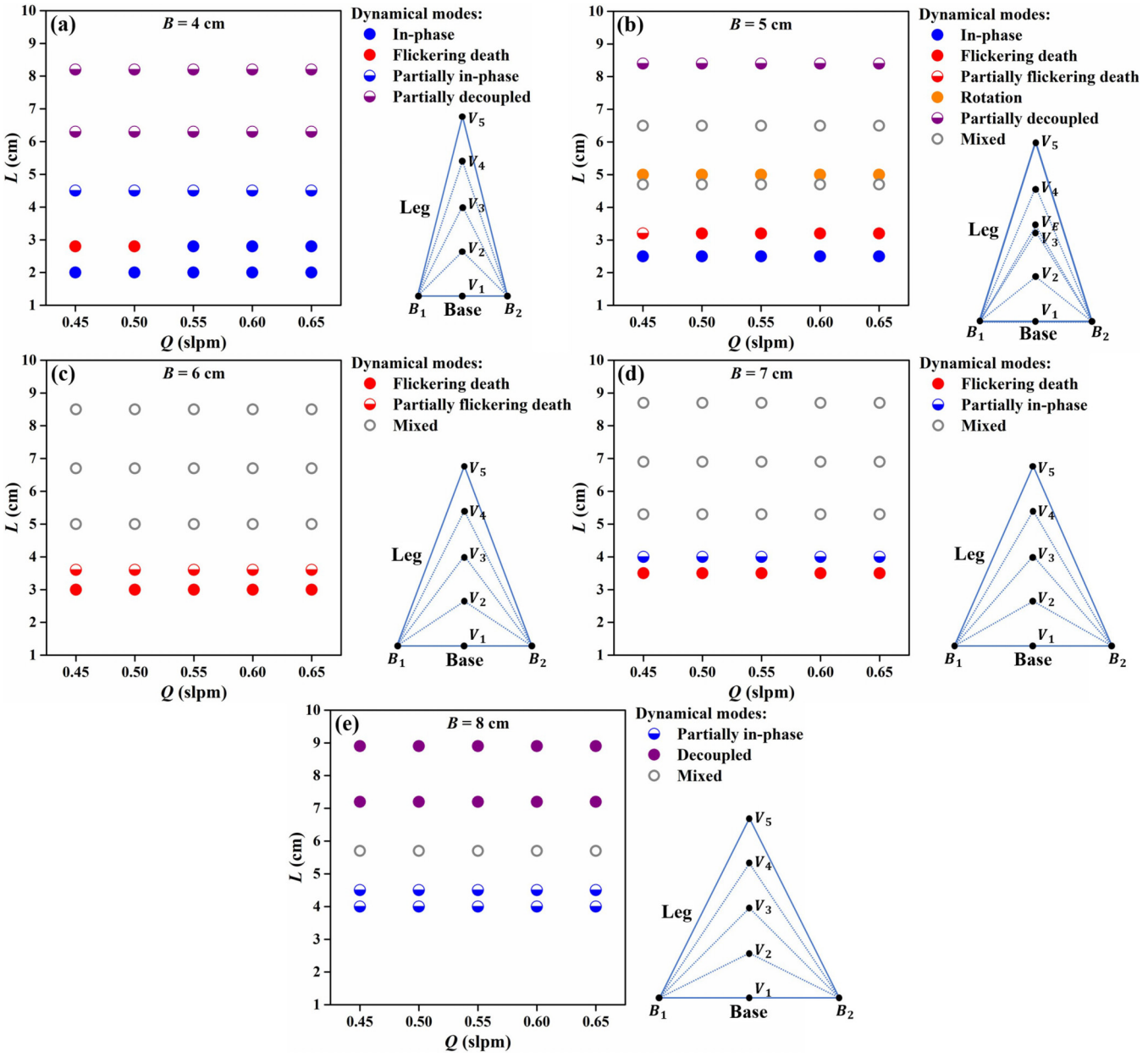

FIG. 6. Experimentally identified dynamical modes for the triple flickering flames system in isosceles triangles with five bases of (a) 4 cm, (b) 5 cm, (c) 6 cm, (d) 7 cm, and (e) 8 cm.

the results of mode recognition for the triple flickering flames system were described in detail below.

When the base is fixed at $B = 4$ cm, four dynamical modes were observed by adjusting L and Q. When the three flames were arranged in a straight line ($L = B/2 = 2$ cm), the in-phase mode appeared. The flickering death mode occurs when the L sightly increases to 2.8 cm. With the increasing fuel flow rate ($Q = 0.55$ slpm or above), the flickering death mode would develop into the in-phase mode. When the L increases to 4.5 cm, the partially in-phase mode appears. The partially decoupled mode is found while L keeps on increasing ($L =$ 6.3 cm or above).

When the base is fixed at $B = 5$ cm, five dynamical modes were observed by adjusting L and Q. When the three flames were arranged in a straight line ($L = B/2 = 2.5$ cm), the in-phase mode appeared. The partially flickering death mode occurs when the L sightly increases to 3.2 cm. With the increase of fuel flow rate ($Q = 0.50$ slpm or above), the partially flickering death mode would change to the flickering death mode. The rotation mode appears if the three flames are arranged in an equal-lateral triangle ($L = 5$ cm). The partially decoupled mode is observed while L increases to 8.4 cm or above. It should be noted that the mixed mode generally occurs between two distinct dynamical modes due to the occurrence of "intermittent" behaviors which means the distinct mode can only maintain for a very short period and then transition to another distinct mode.

When the base is fixed at $B = 6$ cm, three dynamical modes were observed by adjusting L and Q. When the three flames were arranged in a straight line ($L = B/2 = 3$ cm), the

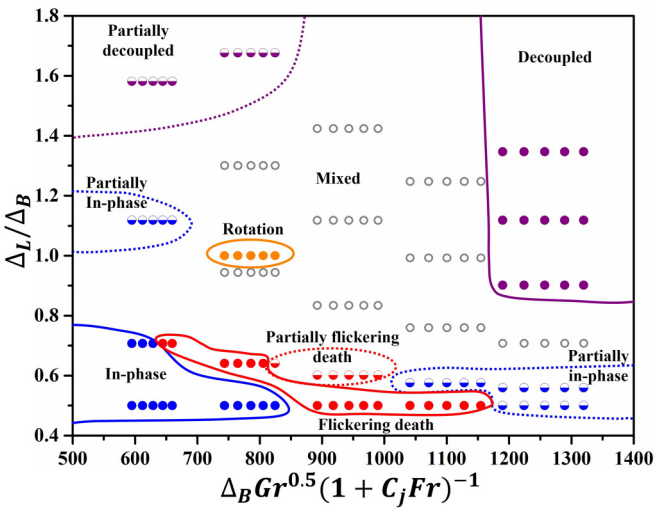

FIG. 7. Regime nomogram of dynamical modes for the triple flickering flames system in isosceles triangles.

flickering death mode appeared. The partially flickering death mode occurs when the L sightly increases to 3.6 cm. The mixed mode occurs as the L continues to increase.

When the base is fixed at $B = 7$ cm, three dynamical modes were observed by adjusting L and Q. When the three flames were arranged in a straight line ($L = B/2 = 3.5$ cm), the flickering death mode appeared. The partially in-phase mode occurs when the L sightly increases to 4.0 cm. The mixed mode also occurs as the L continues to increase.

When the base is fixed at $B = 8$ cm, three dynamical modes were observed by adjusting L and Q. The partially in-phase mode occurs at $L = 4.0$ cm (straight-line arrangement) and $L = 4.5$ cm. The decoupled mode appears while L increases to 7.2 cm or above. The mixed mode generally occurs between the partially in-phase and decoupled modes.

Based on the above results of dynamical mode recognition in physical space, we obtained the regime nomogram in the four dimensionless parameters space (Gr, Fr, Δ_B, and Δ_L). Specifically, the Grashof number defined as $\mathrm{Gr} = gD^3/v_A^2$ is around $O(10^4)$ to represent the buoyance effects, and the Froude number defined as $\mathrm{Fr} = V^2/gD$ varies from 0.09 to 0.19 to represent the fuel flow convention, where V is the bulk velocity, $v_A = 1.56 \times 10^{-5}$ m^2/s is the kinematic viscosity of air at 25°, and $g = 9.8$ m^2/s is the gravitational constant. In addition, the arrangement of the triple flickering flames in an isosceles triangle can be characterized by the dimensionless base ($\Delta_B = B/D = 4.0 \sim 8.0$) and leg ($\Delta_L = L/D = 2.0 \sim 10.8$). Based on the previous study [20] on dual flickering flames, we found that $\alpha \mathrm{Gr}^{0.5}$ is an appropriate parameter for characterizing the dynamical modes, where the dimensionless parameter (α) is the ratio of gap distance and the characteristic length. In addition, $(1 + C_j \mathrm{Fr})^{-1}$ is a correction term to account for the influence of the fuel flow rate, where C_j is a correction coefficient and $C_j = 1.2$ in the present study. Due to the relatively small variation range of Fr ($0.09 \sim 0.19$), it does not play an important role in mode variation in the present study.

It is seen that, as shown in Fig. 7, for a given Δ_B and Fr, the in-phase mode (in the bottom left), partially decoupled mode (in the upper left), the flickering death mode and partially flickering death mode (in the bottom center), the partially in-phase mode (in the middle left and bottom right), and the decoupled mode (in the upper right) are observed with increasing Δ_L. For a given Δ_L, it also found that a similar phenomenon with increasing Δ_B and Fr. Besides, it should be noted that there is a larger mixed region, where many cases that are characterized as mixed mode (intermittent behavior) are between the distinct modes. Therefore, it should also be emphasized that the mixed mode is more common than the distinct modes, and further recognition of the mixed mode merits future studies.

C. Kuramoto model

We first adopted the Kuramoto model to interpret the dynamical modes experimentally observed in the present study. Because the triple flame oscillators were arranged in an isosceles triangle, the coupling strengths between the base flames (flame 1 and flame 2) and the vertex flame (flame 3) are identical. Therefore, we can assume that the coupling strength of the two base flames is equal to K_1 and the coupling strengths of the two base flames and vertex flame are equal to K_2. The governing equations of the Kuramoto model of the triple flickering flame oscillators can be expressed as

$$\dot{\theta}_1(t) = \omega_1 + \frac{K_2}{3}\sin[\theta_3(t) - \theta_1(t)] + \frac{K_1}{3}\sin[\theta_2(t) - \theta_1(t)], \tag{9a}$$

$$\dot{\theta}_2(t) = \omega_2 + \frac{K_2}{3}\sin[\theta_3(t) - \theta_2(t)] + \frac{K_1}{3}\sin[\theta_1(t) - \theta_2(t)], \tag{9b}$$

$$\dot{\theta}_3(t) = \omega_3 + \frac{K_2}{3}\sin[\theta_1(t) - \theta_3(t)] + \frac{K_2}{3}\sin[\theta_2(t) - \theta_3(t)]. \tag{9c}$$

We let $\varphi_{31}(t) = \theta_3(t) - \theta_1(t)$ and $\varphi_{32}(t) = \theta_3(t) - \theta_2(t)$ representing the phase difference between the vertex flame (flame 3) and the two base flames (flame 1 and flame 2), $\varphi_{12}(t) = \theta_1(t) - \theta_2(t)$ representing the phase difference between the two base flames (flame 1 and flame 2). Therefore, the Eqs. (9a)–(9c) can be easily reduced to a two-dimensional system as follows:

$$\dot{\varphi}_{31}(t) = \Delta_{3-1} + \frac{K_1}{3}\sin[\varphi_{12}(t)] - \frac{K_2}{3}\{\sin[\varphi_{32}(t)] + 2\sin[\varphi_{31}(t)]\}, \tag{10a}$$

$$\dot{\varphi}_{32}(t) = \Delta_{3-2} - \frac{K_1}{3}\sin[\varphi_{12}(t)] - \frac{K_2}{3}\{\sin[\varphi_{31}(t)] + 2\sin[\varphi_{32}(t)]\}, \tag{10b}$$

where $\Delta_{31} = \omega_3 - \omega_1$ and $\Delta_{32} = \omega_3 - \omega_2$ are the differences in the natural frequencies between the vertex flame (flame 3) and the two base flames (flame 1 and flame 2). In the present study, we assumed that the three flickering flame oscillators are identical with the same natural frequency, so we have $\Delta_{31} = \Delta_{32} = 0$. Four equilibrium solutions can be obtained

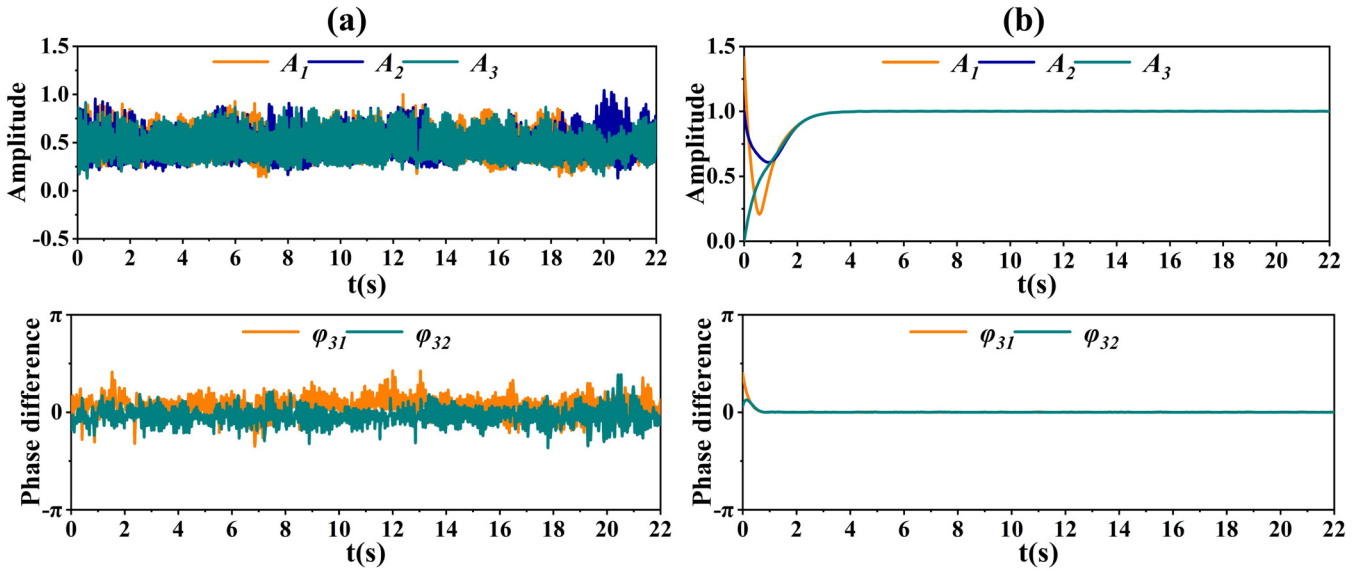

FIG. 8. Instantaneous amplitude and phase difference of (a) experimental and (b) numerical results (Stuart-Landau model) for the in-phase mode.

from Eqs. (10a) and (10b) in the arrangement of the isosceles triangle, and these four solutions represent two dynamical modes, the in-phase and partially in-phase modes, observed in our experiment:

$$\varphi_{31}(t) = \varphi_{32}(t) = \varphi_{12}(t) = 0, \tag{11a}$$

$$\varphi_{31}(t) - \pi = \varphi_{32}(t) - \pi = \varphi_{12}(t) = 0, \tag{11b}$$

$$\varphi_{31}(t) - \pi = \varphi_{32}(t) = \varphi_{12}(t) - \pi = 0, \tag{11c}$$

$$\varphi_{31}(t) = \varphi_{32}(t) - \pi = \varphi_{12}(t) - \pi = 0. \tag{11d}$$

Equation (11a) means that there is no phase difference between the three flickering flame oscillators, corresponding to Mode I: the in-phase mode. Eqs. (11b)–(11d) indicates that two of the three flickering flame oscillators have a phase difference of 0, and the phase difference between these two flame oscillators and the remaining one is π, corresponding to Mode IV: the partially in-phase mode.

If three flickering flame oscillators were arranged in an equilateral triangle, the coupling strength between any two flame oscillators would be the same and denoted as $K_1 = K_2 = K$. Therefore, Eqs. (10a) and (10b) can be rewritten as

$$\dot{\varphi}_{31}(t) = \Delta_{31} + \frac{K}{3}\{\sin[\varphi_{12}(t)] - \sin[\varphi_{32}(t)] - 2\sin[\varphi_{31}(t)]\}, \tag{12a}$$

$$\dot{\varphi}_{32}(t) = \Delta_{32} - \frac{K}{3}\{\sin[\varphi_{12}(t)] + \sin[\varphi_{31}(t)] + 2\sin[\varphi_{32}(t)]\}. \tag{12b}$$

Two additional equilibrium solutions can be obtained from Eqs. (12a) and (12b) as follows:

$$\varphi_{31}(t) = -\varphi_{32}(t) = \varphi_{12}(t) = \frac{2\pi}{3}, \tag{13a}$$

$$\varphi_{31}(t) = -\varphi_{32}(t) = \varphi_{12}(t) = \frac{4\pi}{3}, \tag{13b}$$

which represent the phase differences between any two flickering flame oscillators equal to $2\pi/3$ (or $4\pi/3$), corresponding to Mode V: the rotation mode.

The absence of the flickering death mode and the partially flickering death mode is because the Kuramoto model only characterizes the information of phase but does not contain any information about the amplitude.

D. Complexified Stuart-Landau model

The complexified Stuart-Landau model, as shown in Eq. (7), was numerically investigated by employing the fourth-order Runge-Kutta scheme with the time-step of 0.01 after the separation of the real part from the imaginary part, $z_j = \tilde{\mathcal{B}}_j(t) + i\tilde{\mathcal{B}}_j H(t)$. In Eq. (8), the natural frequency ω_1, ω_2, and ω_3 are set to be unity because the three flickering flame oscillators are considered identical. In addition, α and β are also set to be unity representing that the original amplitude of each flame oscillator is equal to 1. It should be noted that the random initial condition was found to not affect the results of dynamical modes obtained from the model. Five distinct dynamical modes were found by adjusting the complex coupling strength $K = K_{jk} + iK'_{jk}$. It is worth noting that Mode VI: the partially decoupled mode and Mode VII: the decoupled mode are irrelevant to the present study because they are not considered as a globally coupled nonlinear system. The comparison results of instantaneous amplitude and phase difference for the five distinct dynamical modes between the experiment and the complexified Stuart-Landau model are described in detail below.

For Mode I: the in-phase mode (e.g., $K_{31} = K_{32} = 1 + 1i$ and $K_{12} = 2 + 2i$), as shown in Fig. 8, the phase differences (φ_{31} and φ_{32}) fluctuates around zero, and so does the φ_{12}. In addition, the amplitudes (A_1, A_2, and A_3) of the three flame oscillators are much greater than zero. The numerical results from the complexified Stuart-Landau model agree well with the experimental results, namely the phase differences

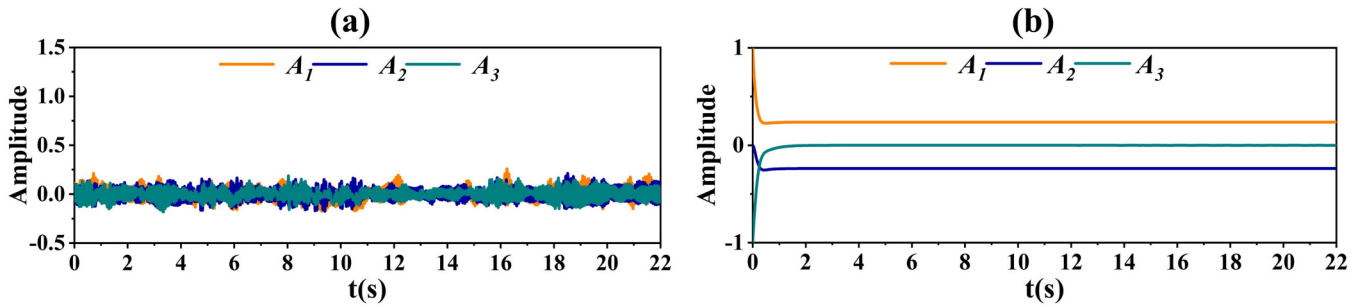

FIG. 9. Instantaneous amplitude and phase difference of (a) experimental and (b) numerical results (Stuart-Landau model) for the flickering death mode.

between the three flames are nearly zero and the amplitudes are around 1.0.

For Mode II: the flickering death mode (e.g., $K_{31} = K_{32} = 3 + 3i$ and $K_{12} = -2-1i$), as shown in Fig. 9, we can see the amplitudes (A_1, A_2, and A_3) of the three flame oscillators are close to zero in both the experimental and numerical results.

For Mode III: the partially flickering death mode (e.g., $K_{31} = K_{32} = 2 + 1i$ and $K_{12} = -2-1i$), as shown in Fig. 10, in both the experimental and numerical results, the amplitude of flame oscillator 3 (A_3) is around zero meaning that flame oscillator 3 exhibits amplitude death mode whereas the phase difference between two base flame oscillators (φ_{12}) is around π indicating that antiphase synchronization happened.

For Mode IV: the partially in-phase mode (e.g., $K_{31} = K_{32} = -3 + 3i$ and $K_{12} = -2-1i$), as shown in Fig. 11, the phase differences (φ_{31} and φ_{32}) are around π indicating that flame 1 and flame 2 exhibit antiphase synchronization with flame 3. It can be easily deduced that the φ_{12} ($\varphi_{12} = \varphi_{32} - \varphi_{31} = 0$) is around zero, indicating that flame 1 and flame 2 exhibit in-phase mode with flame 3.

For Mode V: the rotation mode (e.g., $K_{31} = K_{32} = K_{12} = -2 + 2i$), the average phase differences (φ_{13} and φ_{32}) are around $2\pi/3$, and φ_{21} equals to $2\pi/3$ can be easily deducted, as shown in Fig. 12, indicating that the whole system exhibits rotation mode in both experimental findings and numerical results.

To better illustrate our model results, we calculated two-parameter bifurcation diagrams of synchronization modes, which vary with the real K_{jk} and imaginary K'_{jk}. As shown in Fig. 13(a), to mimic the triple-flame system in an equilateral arrangement, three coupling strengths are set as the same ($K_{12} + iK'_{12} = K_{13} + iK'_{13} = K_{23} + iK'_{23} = K_1 + iK_2$) in the complexified Stuart-Landau model. We found that the mode transition from in-phase mode ($K_1 < 0$) to the rotation mode ($K_1 > 0$) occurs at the bifurcation parameter $K_1 = 0$.

As shown in Fig. 14(a), to mimic the triple-flame system in the isosceles triangle arrangement in our experiment, the coupling strength between two base flames (flame oscillator 1, flame oscillator 2) is fixed, for example, $K_{12} + iK'_{12} = -2-1i$ (Similar bifurcation diagram can be obtained for an arbitrary choice, as shown in the Supplemental Material [62]), while the coupling strength between the vertex flame (flame oscillator 3) and two base flames are set as the same $K_{13} + iK'_{13} = K_{23} + iK'_{23} = K_1 + iK_2$. We found that the mode transition from partially

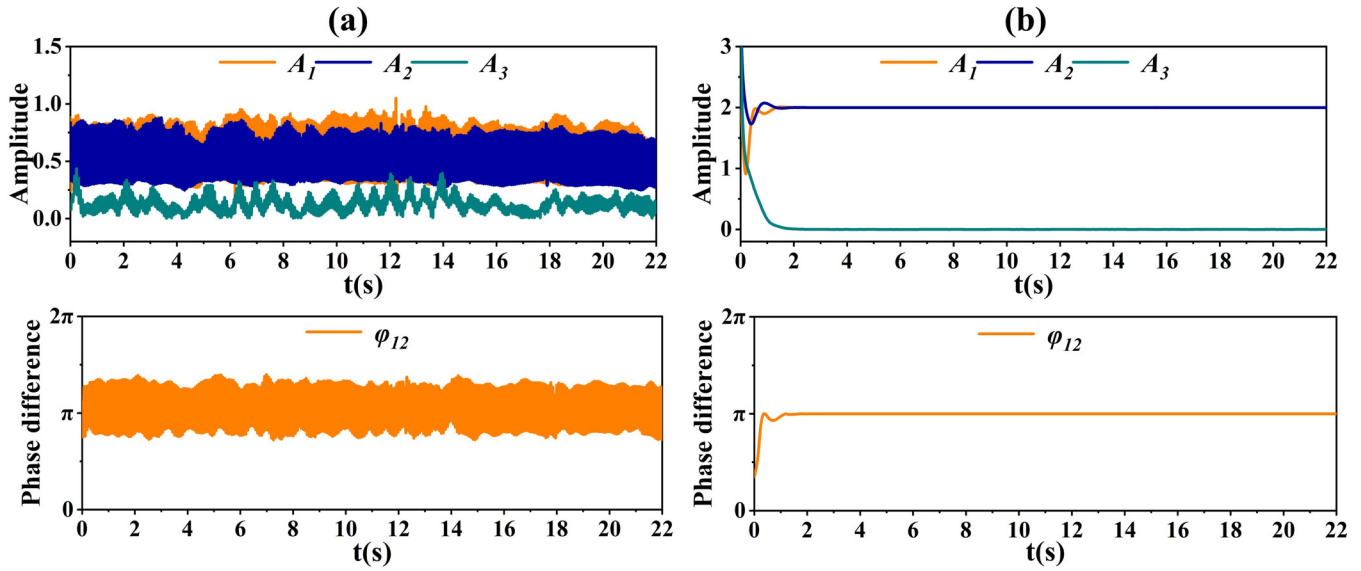

FIG. 10. Instantaneous amplitude and phase difference of (a) experimental and (b) numerical results (Stuart-Landau model) for the partially flickering death mode.

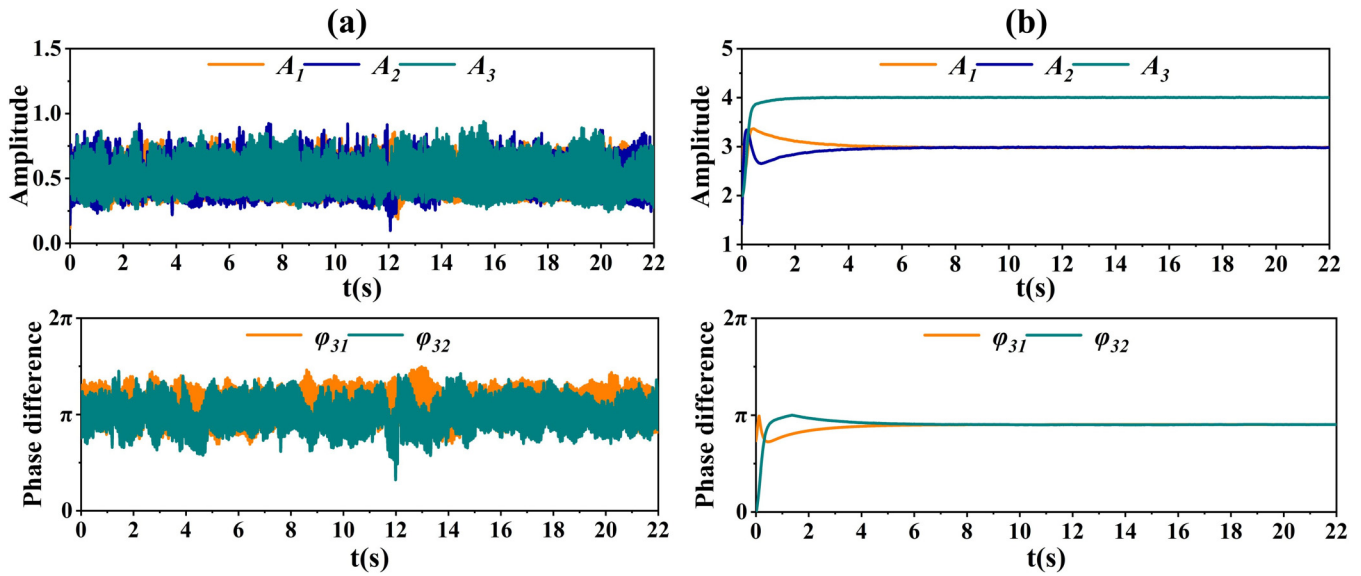

FIG. 11. Instantaneous amplitude and phase difference of (a) experimental and (b) numerical results (Stuart-Landau model) for the partially in-phase mode.

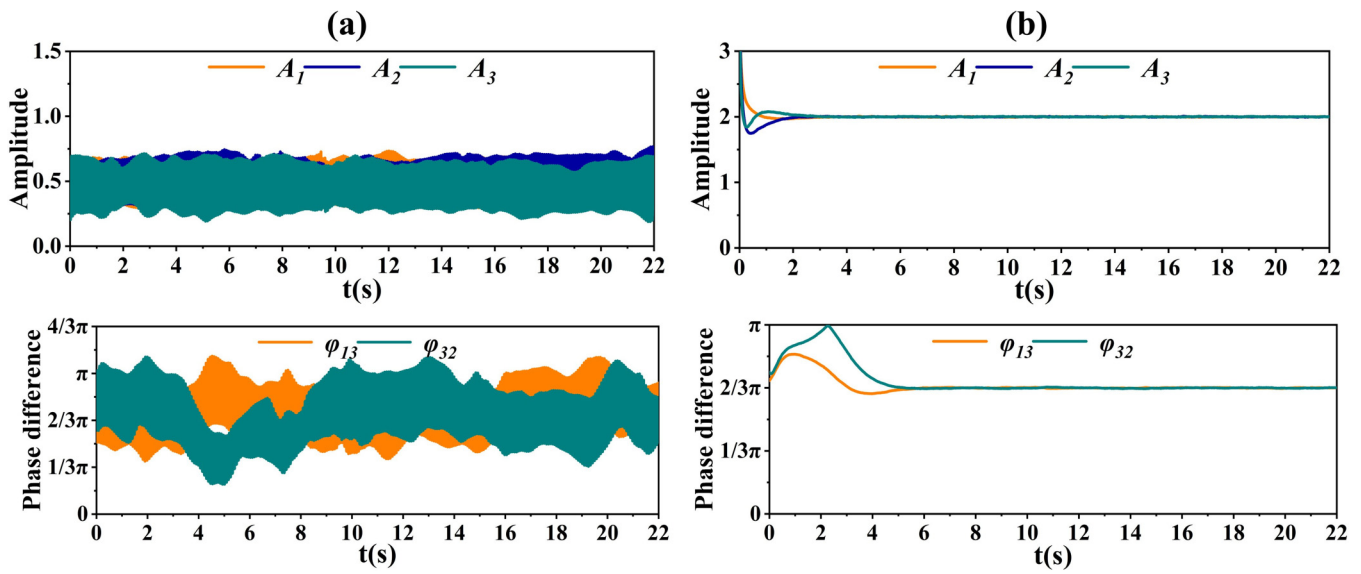

FIG. 12. Instantaneous amplitude and phase difference of (a) experimental and (b) numerical results (Stuart-Landau model) for the rotation mode.

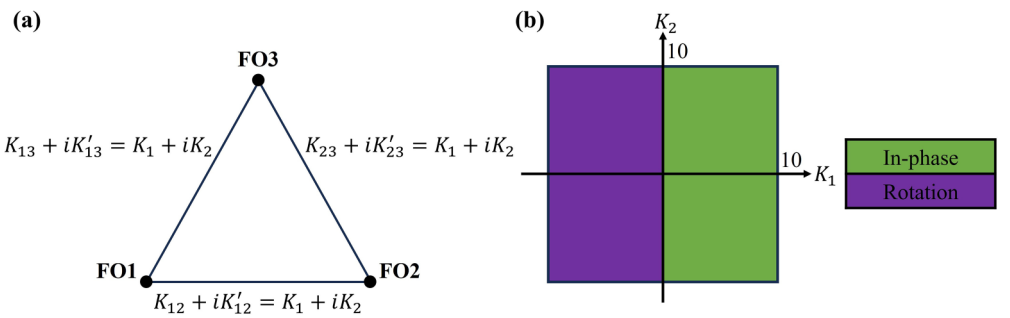

FIG. 13. (a) Schematic for the choice of coupling parameter in an equilateral triangle arrangement. (b) Two-parameter bifurcation diagram of synchronization modes for triple-flame oscillator system in an equilateral triangle arrangement.

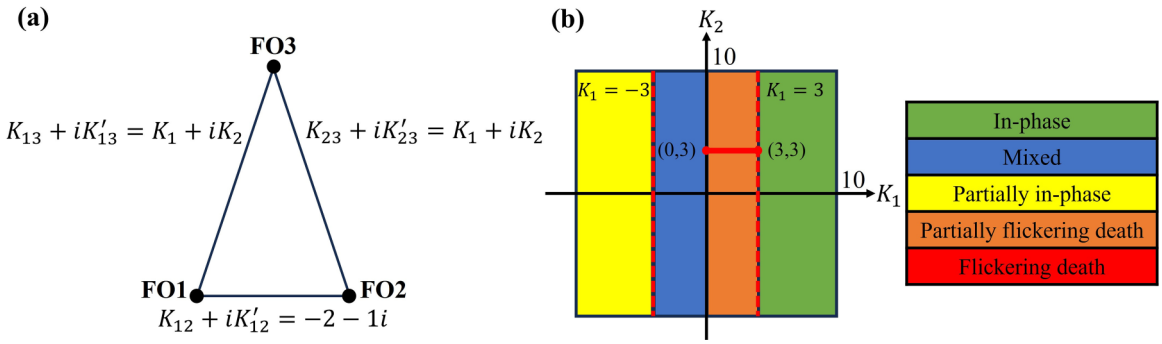

FIG. 14. (a) Schematic for the choice of coupling parameter in an isosceles triangle arrangement. (b) Two-parameter bifurcation diagram of synchronization modes for triple-flame oscillator system in an isosceles triangle arrangement.

in-phase mode ($K_1 < -3$) to mixed mode ($-3 < K_1 < 0$) at the bifurcation parameter $K_1 = -3$; from mixed mode to partially flickering death mode ($0 < K_1 < 3$) at the bifurcation parameter $K_1 = 0$; from partially flickering death mode to partially in-phase mode ($K_1 > 3$) at the bifurcation parameter $K_1 = 3$. Flickering death mode occurs when the coupling strength K_1, K_2 satisfy $(K_1, K_2) \in \{0 \leqslant K_1 \leqslant 3,\ K_2 = 3\}$.

The blue zone is identified as a "mixed mode" due to the phase differences between the flame oscillators not remaining as a constant, and this is consistent with the definition of the "mixed mode" given in the previous article: the intermittent behavior between the two pure distinct dynamical modes. In addition, we found that the frequency of the flame oscillators in the different dynamical modes is dominated by the imaginary part of the coupling strength K_2, that is, the frequencies of flame oscillators are proportional to the absolute value of K_2.

So far, five distinct dynamical modes (in-phase, flickering death, partially flickering death, partially in-phase, and rotation modes) observed in our experiment were successfully reproduced by the complexified Stuart-Landau model, and two-parameter bifurcation diagrams Figs. 13(b) and 14(b) indicate that the occurrence of the dynamical modes in the complexified Stuart-Landau model is not just accidental, the distinct dynamical modes take up certain areas in the bifurcation diagram and have clear boundaries. The transition between the emerging dynamical modes is governed by the bifurcation coupling strength $K = K_{jk} + iK'_{jk}$, consistent with the finding in our experiment that the change of the experimental parameters (flue flow rate Q and distance d) will lead to the transition of the dynamical modes. Establishing the relationship between the coupling strength and the experimental parameters merits future studies because we must develop a phenomenological model and compare its dynamical behaviors with the Stuart-Landau model.

The innovation and advancement of the complexified Stuart-Landau model are mainly reflected in the following two aspects: On the one hand, the complexified Stuart-Landau model poses a new possibility to cause the amplitude death modes in globally coupled nonlinear dynamical systems consisting of identical oscillators barely through the introduction of the complex coupling strength, which is a more natural and simple way. On the other hand, compared with the early studies [26,27], the complexified Stuart-Landau model can better distinguish the dynamical modes through precise calculation of the instantaneous amplitude and phase difference information.

IV. CONCLUDING REMARKS

The triple-flame system is a key component in many multiple-flame systems, due to strong interactions for the nearest flames. In the present study, we adopted a well-controlled gas-fuel diffusion flame experiment platform to systematically investigate a triple-flame system of flickering flames in isosceles triangles by adjusting the flame distances (B and L) and the fuel flow rate (Q). Seven synchronization modes, in-phase, flickering death, partially flickering death, partially in-phase, rotation, partially decoupled, and decoupled modes, were experimentally observed and identified. For first the time, we established a regime nomogram for the dynamical modes of the triplet-flame system in the Δ_L/Δ_B and $\Delta_B \mathrm{Gr}^{0.5}(1 + C_j \mathrm{Fr})^{-1}$ space, which is helpful in further understanding the physical mechanisms of complex multiflame systems.

The Kuramoto model and the complexified Stuart-Landau model were adopted to qualitatively interpret the dynamical modes exhibited in our experiments from the perspective of nonlinear dynamics. For the Kuramoto model, the in-phase, partially in-phase, and rotation modes are reproduced theoretically by obtaining the equilibrium solutions of the governing equations. For the complexified Stuart-Landau model, including the modes predicted by the Kuramoto model, the flickering death and partially flickering death modes are reproduced very well.

In addition, we fully recognized two potential focuses in future works: first, the extensive application of complexified parameters such as natural frequency ω_j and amplitude coefficient α and β, and the association of these parameters to the physical parameter in real-world nonlinear dynamical systems are to be investigated. Such endeavors will expand our perspective on nonlinear dynamics, thereby initiating our research position to complexified network dynamics and establishing a connection between these theories and real-world physics. Second, more flame-oscillator experiments are to be carried out with a broader range of parameter settings to discover the potential new dynamical modes and the application of a turbulent flame oscillator, which is closer to the practical combustor, for example, the annular combustor of gas-turbine engines.

The data that support the findings of this study are available from the corresponding author upon reasonable request.

ACKNOWLEDGMENTS

This work is financially supported by the National Natural Science Foundation of China (No. 52176134) and partially by the APRC - CityU New Research Initiatives/Infrastructure Support from Central of City University of Hong Kong (No. 9610601).

The authors declare that they have no known competing financial interests or personal relationships that could have appeared to influence the work reported in the paper.

[1] Y. Kuramoto, *Chemical Oscillations, Waves, and Turbulence* (Springer Science & Business Media, New York, 2012).

[2] S. H. Strogatz, *Nonlinear Dynamics and Chaos with Student Solutions Manual: With Applications to Physics, Biology, Chemistry, and Engineering* (CRC Press, Boca Raton, FL, 2018).

[3] D. S. Chamberlin and A. Rose, The flicker of luminous flames, Proc. Combust. Inst **1-2**, 27 (1948).

[4] J. Barr, Diffusion flames, Symp. (Int.) Combust. **4**, 765 (1953).

[5] W. M. G. Malalasekera, H. K. Versteeg, and K. Gilchrist, A review of research and an experimental study on the pulsation of buoyant diffusion flames and pool fires, Fire Mater. **20**, 261 (1996).

[6] S. R. Tieszen, On the fluid mechanics of fires, Annu. Rev. Fluid Mech. **33**, 67 (2001).

[7] D. Durox, T. Yuan, F. Baillot, and J. Most, Premixed and diffusion flames in a centrifuge, Combust. Flame **102**, 501 (1995).

[8] N. Fujisawa and T. Okuda, Effects of co-flow and equivalence ratio on flickering in partially premixed flame, Int. J. Heat Mass Transf. **121**, 1089 (2018).

[9] L.-D. Chen, J. Seaba, W. Roquemore, and L. Goss, Buoyant diffusion flames, Proc. Combust. Inst. **22**, 677 (1989).

[10] D. Moreno-Boza, W. Coenen, J. Carpio, A. L. Sánchez, and F. A. Williams, On the critical conditions for pool-fire puffing, Combust. Flame **192**, 426 (2018).

[11] D. Moreno-Boza, W. Coenen, A. Sevilla, J. Carpio, A. Sánchez, and A. Liñán, Diffusion-flame flickering as a hydrodynamic global mode, J. Fluid Mech. **798**, 997 (2016).

[12] H. Kitahata, J. Taguchi, M. Nagayama, T. Sakurai, Y. Ikura, A. Osa, Y. Sumino, M. Tanaka, E. Yokoyama, and H. Miike, Oscillation and synchronization in the combustion of candles, J. Phys. Chem. A **113**, 8164 (2009).

[13] D. M. Forrester, Arrays of coupled chemical oscillators, Sci. Rep. **5**, 1 (2015).

[14] K. Manoj, S. A. Pawar, and R. Sujith, Experimental evidence of amplitude death and phase-flip bifurcation between in-phase and antiphase synchronization, Sci. Rep. **8**, 11626 (2018).

[15] X. Ju, A. Bunkwang, T. Yamazaki, T. Matsuoka, and Y. Nakamura, Flame flickering can cease under normal gravity and atmospheric pressure in a horizontally moving dual burner system, Phys. Rev. Appl. **19**, 014060 (2023).

[16] S. Dange, S. A. Pawar, K. Manoj, and R. Sujith, Role of buoyancy-driven vortices in inducing different modes of coupled behaviour in candle-flame oscillators, AIP Adv. **9**, 015119 (2019).

[17] N. Fujisawa, K. Imaizumi, and T. Yamagata, Synchronization of dual diffusion flame in co-flow, Exp. Therm. Fluid Sci. **110**, 109924 (2020).

[18] A. Bunkwang, T. Matsuoka, and Y. Nakamura, Similarity of dynamic behavior of buoyant single and twin jet-flame (s), J. Therm. Sci. Technol. **15**, 1 (2020).

[19] A. Bunkwang, T. Matsuoka, and Y. Nakamura, Mode transition of interacting buoyant nonpremixed flames, J. Therm. Sci. Technol. **15**, 1 (2020).

[20] T. Yang, X. Xia, and P. Zhang, Vortex-dynamical interpretation of antiphase and in-phase flickering of dual buoyant diffusion flames, Phys. Rev. Fluids **4**, 053202 (2019).

[21] T. Tokami, M. Toyoda, T. Miyano, I. T. Tokuda, and H. Gotoda, Effect of gravity on synchronization of two coupled buoyancy-induced turbulent flames, Phys. Rev. E **104**, 024218 (2021).

[22] K. Okamoto, A. Kijima, Y. Umeno, and H. Shima, Synchronization in flickering of three-coupled candle flames, Sci. Rep. **6**, 36145 (2016).

[23] T. Yang, Y. Chi, and P. Zhang, Vortex interaction in triple flickering buoyant diffusion flames, Proc. Combust. Inst. **39**, 1893 (2022).

[24] Y. Chi, T. Yang, and P. Zhang, Dynamical mode recognition of triple flickering buoyant diffusion flames in Wasserstein space, Combust. Flame **248**, 112526 (2023).

[25] D. M. Abrams and S. H. Strogatz, Chimera states for coupled oscillators, Phys. Rev. Lett. **93**, 174102 (2004).

[26] K. Manoj, S. A. Pawar, S. Dange, S. Mondal, R. Sujith, E. Surovyatkina, and J. Kurths, Synchronization route to weak chimera in four candle-flame oscillators, Phys. Rev. E **100**, 062204 (2019).

[27] K. Manoj, S. A. Pawar, and R. Sujith, Experimental investigation on the susceptibility of minimal networks to a change in topology and number of oscillators, Phys. Rev. E **103**, 022207 (2021).

[28] T. Chen, X. Guo, J. Jia, and J. Xiao, Frequency and phase characteristics of candle flame oscillation, Sci. Rep. **9**, 342 (2019).

[29] A. Gergely, B. Sándor, C. Paizs, R. Tötös, and Z. Néda, Flickering candle flames and their collective behavior, Sci. Rep. **10**, 21305 (2020).

[30] T. Yang and P. Zhang, Faster flicker of buoyant diffusion flames by weakly rotatory flows, Theor. Comput. Fluid Dyn. **37**, 781 (2023).

[31] T. Yang, Y. Ma, and P. Zhang, Dynamical behaviors of small-scale buoyant diffusion flame oscillators in externally swirling flows, arXiv:2303.15789.

[32] X. Xia and P. Zhang, A vortex-dynamical scaling theory for flickering buoyant diffusion flames, J. Fluid Mech. **855**, 1156 (2018).

[33] H. Sato, K. Amagai, and M. Arai, Diffusion flames and their flickering motions related with Froude numbers under various gravity levels, Combust. Flame **123**, 107 (2000).

[34] B. M. Cetegen and T. A. Ahmed, Experiments on the periodic instability of buoyant plumes and pool fires, Combust. Flame **93**, 157 (1993).
[35] M. Aravind, I. Tiwari, V. Vasani, J.-M. Cruz, D. A. Vasquez, and P. Parmananda, Ethanol lamp: A simple, tunable flame oscillator and its coupled dynamics, Eur. Phys. J.: Spec. Top. **231**, 179 (2022).
[36] A. Gergely, C. Paizs, R. Tötös, and Z. Néda, Oscillations and collective behavior in convective flows, Phys. Fluids **33**, 124104 (2021).
[37] M. Sezgin and B. l. Sankur, Survey over image thresholding techniques and quantitative performance evaluation, J. Electron. Imaging **13**, 146 (2004).
[38] N. Otsu, A threshold selection method from gray-level histograms, IEEE Trans. Syst. Man Cybern. **9**, 62 (1979).
[39] M. Rosenblum and J. Kurths, *Synchronization: A Universal Concept in Nonlinear Science* (Cambridge University Press, Cambridge, 2003).
[40] A. T. Winfree, Biological rhythms and the behavior of populations of coupled oscillators, J. Theor. Biol. **16**, 15 (1967).
[41] Y. Kuramoto, *New* (Springer, Berlin, 1984).
[42] J. Buck and E. Buck, Mechanism of rhythmic synchronous flashing of fireflies: Fireflies of southeast asia may use anticipatory time-measuring in synchronizing their flashing, Science **159**, 1319 (1968).
[43] T. Antonsen Jr, R. Faghih, M. Girvan, E. Ott, and J. Platig, External periodic driving of large systems of globally coupled phase oscillators, Chaos **18**, 037112 (2008).
[44] F. C. Hoppensteadt and E. M. Izhikevich, *Weakly Connected Neural Networks* (Springer Science & Business Media, New York, 1997).
[45] F. Dörfler, M. Chertkov, and F. Bullo, Synchronization in complex oscillator networks and smart grids, Proc. Natl. Acad. Sci. USA **110**, 2005 (2013).
[46] G. Ermentrout and N. Kopell, Oscillator death in systems of coupled neural oscillators, SIAM J. Appl. Math. **50**, 125 (1990).
[47] Y. Zhang, J. L. Ocampo-Espindola, I. Z. Kiss, and A. E. Motter, Random heterogeneity outperforms design in network synchronization, Proc. Natl. Acad. Sci. USA **118**, e2024299118 (2021).
[48] W. Zou, D. Senthilkumar, R. Nagao, I. Z. Kiss, Y. Tang, A. Koseska, J. Duan, and J. Kurths, Restoration of rhythmicity in diffusively coupled dynamical networks, Nat. Commun. **6**, 7709 (2015).
[49] B. Kuntsevich and A. Pisarchik, Synchronization effects in a dual-wavelength class-B laser with modulated losses, Phys. Rev. E **64**, 046221 (2001).
[50] S. W. Haugland, A. Tosolini, and K. Krischer, Between synchrony and turbulence: Intricate hierarchies of coexistence patterns, Nat. Commun. **12**, 5634 (2021).
[51] G. Vathakkattil Joseph and V. Pakrashi, Limits on antiphase synchronization in oscillator networks, Sci. Rep. **10**, 10178 (2020).
[52] H. Hong and S. H. Strogatz, Kuramoto model of coupled oscillators with positive and negative coupling parameters: An example of conformist and contrarian oscillators, Phys. Rev. Lett. **106**, 054102 (2011).
[53] M. Thümler, S. G. Srinivas, M. Schröder, and M. Timme, Synchrony for weak coupling in the complexified Kuramoto model, Phys. Rev. Lett. **130**, 187201 (2023).
[54] G. Saxena, A. Prasad, and R. Ramaswamy, Amplitude death: The emergence of stationarity in coupled nonlinear systems, Phys. Rep. **521**, 205 (2012).
[55] R. E. Mirollo and S. H. Strogatz, Amplitude death in an array of limit-cycle oscillators, J. Stat. Phys. **60**, 245 (1990).
[56] D. G. Aronson, G. B. Ermentrout, and N. Kopell, Amplitude response of coupled oscillators, Phys. D **41**, 403 (1990).
[57] F. M. Atay, Distributed delays facilitate amplitude death of coupled oscillators, Phys. Rev. Lett. **91**, 094101 (2003).
[58] S. H. Strogatz, Death by delay, Nature (London) **394**, 316 (1998).
[59] D. R. Reddy, A. Sen, and G. L. Johnston, Time delay induced death in coupled limit cycle oscillators, Phys. Rev. Lett. **80**, 5109 (1998).
[60] K. Sathiyadevi, V. Chandrasekar, and D. Senthilkumar, Inhomogeneous to homogeneous dynamical states through symmetry breaking dynamics, Nonlinear Dyn. **98**, 327 (2019).
[61] K. Sathiyadevi, V. Chandrasekar, and D. Senthilkumar, Stable amplitude chimera in a network of coupled Stuart-Landau oscillators, Phys. Rev. E **98**, 032301 (2018).
[62] See Supplemental Material at http://link.aps.org/supplemental/10.1103/PhysRevE.109.024211 for the movies of distinct dynamical modes and the bifurcation diagram of synchronization modes.